Global and Planetary Change 122 (2014) 176–185

Contents lists available at ScienceDirect

Global and Planetary Change

journal homepage: www.elsevier.com/locate/gloplacha

Regional moisture change over India during the past Millennium: A comparison of multi-proxy reconstructions and climate model simulations

Stefan Polanski [a,*], Bijan Fallah [a], Daniel J. Befort [a,1], Sushma Prasad [b], Ulrich Cubasch [a]

[a] Institute of Meteorology, Freie Universität Berlin, Carl-Heinrich-Becker-Weg 6-10, 12165 Berlin, Germany
[b] Institute of Earth- and Environmental Science, Universität Potsdam, Karl-Liebknecht-Straße 24-25, 14476 Potsdam, Germany

ARTICLE INFO

Article history:
Received 18 April 2014
Received in revised form 15 August 2014
Accepted 18 August 2014
Available online 26 August 2014

Keywords:
Medieval Climate Anomaly
Little Ice Age
moisture variations in India
atmosphere-only climate model simulations
Lonar Crater Lake
multi-proxy reconstructions

ABSTRACT

The Indian Monsoon Variability during the past Millennium has been simulated with the ECHAM5 model in two different time slices: Medieval Climate Anomaly and the Little Ice Age. The simulations are compared with new centennial-resolving paleo-reconstructions inferred from various well-dated multi-proxies from two core regions, the Himalaya and Central India. A qualitative moisture index is derived from the proxies and compared with simulated moisture anomalies.

The reconstructed paleo-hydrological changes between the Little Ice Age and the Medieval Climate Anomaly depict a dipole pattern between Himalaya and Central India, which is also captured by the model.

In the Medieval Climate Anomaly the model exhibits stronger (weaker) dipole signals during summer (winter) compared to Little Ice Age. In summer (winter) months of "Medieval Climate Anomaly minus Little Ice Age" the model simulates wetter conditions over eastern (western and central) Himalaya. Over Central India, a simulated weakening of Indian Summer Monsoon during warmer climate is coincident with reconstructed drying signal in the Lonar Lake record.

Based on the model simulations, we can differentiate three physical mechanisms which can lead to the moisture anomalies: (i) the western and central Himalaya are influenced by extra-tropical Westerlies during winter, (ii) the eastern Himalaya is affected by summer variations of temperature gradient between Bay of Bengal and Indian subcontinent and by a zonal band of intensified Indian–East Asian monsoon link north of 25°N, and (iii) Central India is dominated by summer sea surface temperature anomalies in the northern Arabian Sea which have an effect on the large-scale advection of moist air masses. The temperatures in the Arabian Sea are linked to the Indo Pacific Warm Pool, which modulates the Indian monsoon strength.

1. Introduction

Long-term climate reconstructions derived from various well-dated proxy data (e.g., Prasad and Enzel, 2006; Fleitmann et al., 2007; Liu et al., 2009; Borgaonkar et al., 2010; Ponton et al., 2012; Prasad et al., 2014) indicate that the past Millennium is the best documented interval with both historical and climate data. It can be divided into two major climate periods: the Medieval Climate Anomaly (ca. 900–1350 AD) and the Little Ice Age (ca. 1500–1850 AD) (e.g., Lamb, 1965; Grove, 1988; Graham et al., 2010). Variations in volcanic forcing coupled with the remote impact of the internal dynamics of climate modes in the oceans such as the El Niño–Southern Oscillation are some of the major drivers contributing to long-term fluctuations in global temperature conditions during the last 1200 years (Jones et al., 2001) whereas solar forcing has been recently found to play a minor role (Schurer et al., 2014). These thermal changes exhibit a strong impact on global and regional climate phenomena as monsoons (Meehl et al., 2009), which arise due to seasonal and latitudinal differences in the incoming solar radiation with effects on the land–sea thermal contrast (Webster et al., 1998; Gadgil, 2003). Consequently, large-scale pressure gradients evolve including strong low-level atmospheric wind circulations (Dallmeyer et al., 2012). Monsoon systems are characterized by a strong spatiotemporal variability from multi-millennial to intra-seasonal time scales (Wang, 2006; Ding, 2007). The Asian Monsoon System is the strongest monsoon system of the world (Clift and Plumb, 2008) and is divided into two strongly non-linear interacting subsystems: the East Asian Monsoon and the Indian Monsoon (Wang et al., 2001). The increased occurrence and frequency of extreme monsoon rainfall events (e.g., Krishnan et al., 2009; Shaw and Nguyen, 2011; Ummenhofer et al., 2012) in recent times has affected the livelihood of more than

* Corresponding author. Tel.: +49 331 8872860.
E-mail address: stefan.polanski@gmx.de (S. Polanski).
[1] School of Geography, Earth and Environmental Sciences, University of Birmingham, UK.

http://dx.doi.org/10.1016/j.gloplacha.2014.08.016

2.5 billion people. Hence, an understanding of the large-scale mechanisms and regional spatiotemporal variations leading to past monsoon changes is crucial for an advanced prediction of the Indian Monsoon (e.g., Krishna Kumar et al., 2005), and to develop proper mitigation strategies in a global warming scenario. Several studies have been already carried out analyzing the Asian monsoon variability during the last Millennium (e.g., Cook et al., 2010; Wang et al., 2010; Sinha et al., 2011a, b). Using a paleoclimatic network approach Rehfeld et al. (2013) found a stronger Indian Summer Monsoon (ISM) circulation and a northward intrusion of the ITCZ during Medieval Warm Period caused by an earlier retreat of the Tibetan High in spring. In colder periods such as Little Ice Age, a more regional influence on the ISM strength has been identified (Rehfeld et al., 2013).

Previous reconstruction studies have mainly focused on the Tibetan Plateau and Central Asia. Until recently only few records were available from the Indian Peninsula. This led to a systematic overemphasis on the role of the Tibetan Plateau and Central Asia on the monsoon, resulting in a gap in understanding the past monsoon changes over India (Wang et al., 2010; Polanski et al., 2012). The combined multi-proxy-climate model approach, as adopted in HIMPAC ("Himalaya: Modern and Past Climates"; http://www.himpac.org) and CADY ("Central Asian Climate Dynamics"; http://www.cady-climate.org) projects, aims at analyzing the past monsoon climate in India during the Holocene. It introduces new, well-dated paleo-records from India, which are based on multiple proxies and archives. A 11,000-year long, high-resolution record from Central India is now available (Anoop et al., 2013; Menzel et al., 2013; Prasad et al., 2014; Sarkar et al., 2014) and presents a unique opportunity for a comparison of long-term climate time proxy series with paleo-model simulations. The Lonar Lake is influenced by both monsoon branches: from the Arabian Sea and the Bay of Bengal (Sengupta and Sarkar, 2006).

Ensemble simulations over the last 1200 years using a comprehensive fully coupled Earth System Model have been performed using external forcing parameters such as solar variations or volcanic activity derived from reconstructions (Jungclaus et al., 2010). Owing to the coarse horizontal resolution of ca. 3.75° × 3.75°, these coupled models are not able to capture regional-scale atmospheric circulation and moisture patterns, which strongly depend on a realistic representation of the local topography (Polanski et al., 2010). In this study, transient time slice experiments are performed for selected episodes of the past using the ECHAM5 model with a spatial resolution of T63 (ca. 1.8° × 1.8°). This improves the simulation of the hydrological cycle in India and the Himalayan region (Anandhi and Nanjundiah, 2014).

In this paper the reconstruction of the relative moisture index and the observational datasets used are presented first (Section 2). Section 3 deals with the simulated and reconstructed monsoon variability during the Medieval Climate Anomaly and the Little Ice Age. In Section 4 the physical mechanisms leading to the monsoon variability are discussed. The main results are summarized in Section 5.

2. Model and data

2.1. Model set-up

A two-step approach is used to simulate the past Millennium: (i) the fully coupled Community Earth System Models (COSMOS) from Max Planck Institute for Meteorology (here referred to AOGCM throughout the paper) with a spatial resolution of T31 (ca. 3.75° × 3.75°) with 19 vertical levels and coupled to the ocean model MPIOM (horizontal resolution of GR3.0 (ca. 3° × 3°)), 40 vertical levels; and (ii) the atmosphere-only general circulation model ECHAM5 (here referred to AGCM throughout the paper) with a spatial resolution of T63 (ca. 1.8° × 1.8°) and 31 vertical levels. Further details about the models can be found in Marsland et al. (2003), Roeckner et al. (2003), Wetzel et al. (2006) and Raddatz et al. (2007).

In the Millennium project (Jungclaus et al., 2010), an ensemble of five simulations covering the time between 800 and 2005 AD have been calculated starting from different ocean initial conditions. The model simulations have been forced by: solar variability (Solanki et al., 2004; Krivova et al., 2007), volcanoes (Crowley et al., 2008), land cover changes (Pongratz et al., 2008), orbital variations (Bretagnon and Francou, 1988), greenhouse gases (Fortuin and Kelder, 1998; Marland et al., 2003), and aerosols (Tanre et al., 1984). A detailed description of the Millennium simulations is documented in Jungclaus et al. (2010). These simulations have been analyzed to detect extreme wet and dry summer monsoon rainfall anomalies over India on centennial time scales.

Fig. 1 illustrates the spatiotemporal evolution of the first leading EOF (Empirical Orthogonal Function) for the reconstructed PDSI from Monsoon Asia Drought Atlas (MADA; Cook et al., 2010) and summer (JJAS) rainfall from the Millennium experiment (Jungclaus et al., 2010). Fig. 1a presents the EOF1 pattern of MADA and the explained variances of the first 10 Principle Components (PCs). Similarly, Fig. 1b shows the EOF1 pattern and explained variances of first 10 PCs of summer (JJAS) rainfall from mil0014 ensemble member of the Millennium experiment. In addition, the summer (JJAS) PC1 time series of rainfall for the five ensemble members of the Millennium experiment from 850 to 1950 AD (Jungclaus et al., 2010) and for the PDSI from MADA from 1300 to 1950 AD are shown in Fig. 1c. The time series are smoothed with a 101-yr moving-average filter. To compare the patterns, MADA is remapped on common T31 grid.

The first leading EOF pattern of MADA is associated with monsoon activity in South and Southeast Asia (Cook et al., 2010). EOF1 of summer rainfall presents similar patterns over India and Central Asia as in MADA (Fig. 1a, b). For the entire period from 1300 to 1900 AD (excluding the increase in CO_2 during past century), PC1 time series of mil0010 experiment show the best agreement with MADA (correlation coefficient = 0.56), but during the selected Little Ice Age epoch (1515–1715 AD), mil0014 has the highest temporal correlation coefficient (0.51) and a similar trend (Fig. 1c). Correlation coefficients between PC1 of other experiments and MADA are mil0010 (−0.07), mil0012 (−0.58), mil0013 (−0.15) and mil0015 (−0.08), respectively. In order to check whether the mil0014 correlation is also significant on longer time scales we additionally compared the 101-yr running means of PC1 time series of simulated PDSI from the Millennium experiment with MADA (Fig. 2) including a long-term LIA period (1400–1900 AD) defined by Mann et al. (1999) and Cronin et al. (2003). The PDSI has been calculated after Dai et al. (2004). The pattern correlations between EOF1 of PDSI from MADA and the Millennium experiments are mil0010 (0.44), mil0012 (0.46), mil0013 (0.51), mil0014 (0.51) and mil0015 (0.54), respectively. Only the PC1 time series of mil0014 member has a significant positive correlation (0.58) with MADA in this longer LIA period. Correlation coefficients between PC1 of other experiments and MADA are mil0010 (−0.53), mil0012 (−0.39), mil0013 (−0.67) and mil0015 (0.12), respectively indicating that mil0014 shows the best performance during the overlapping period (Fig. 2; Fallah and Cubasch, 2014). More supporting information about the model set-up are summarized in the Supplementary material (Figs. S1, S2 and S3).

Limitations in available computing resources have compelled us to focus on a single higher-resolved calculation of the Millennium experiment. Since mil0014 shows best fit to MADA, it has been selected as basis for the AGCM simulation (Supplementary material).

The mil0014 experiment has been simulated with the higher-resolved AGCM for the Medieval Climate Anomaly (MCA; 900–1100 AD) and the Little Ice Age (LIA; 1515–1715 AD). To determine the time and space extension for these two periods, we checked the 200-yr averaged surface temperature anomalies of MCA and LIA summer (JJAS) over the Northern Hemisphere for mil0014 experiment and ensemble average in comparison to their climatological means (800–1899 AD; excluding the 20th century warming). The results show a clear warming up to +0.3 K (cooling up to −0.3 K) compared

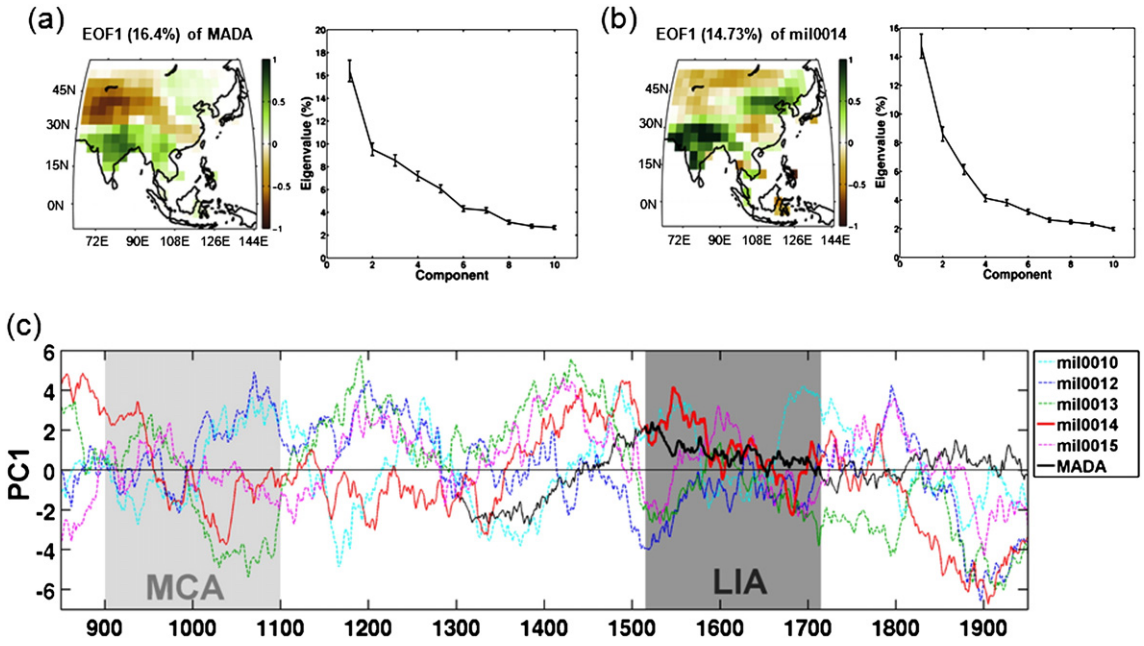

Fig. 1. First leading EOF and its explained variability of 10 leading PCs for PDSI from MADA (Fig. 1a; Cook et al., 2010) and for summer rainfall of mil0014 ensemble member of the Millennium experiment (Fig. 1b; Jungclaus et al., 2010). Fig. 1c: PC1 time series of summer precipitation (JJAS; mm/year) as 101-yr running mean for the five ensemble members of the Millennium experiment from 805 to 1995 AD and for the PDSI from MADA (solid black line) from 1300 to 1995 AD. The mil0014 experiment (solid red line) has been used to drive our AGCM experiments. During the LIA mil0014 (thick red line) has, in comparison to all the other ensemble members, the highest temporal correlation (0.51) to MADA (thick black line) and a similar trend. The selection of time slices for our AGCM simulations are shown by the boxes for the Medieval Climate Anomaly (MCA; 900–1100 AD) in light gray and the Little Ice Age (LIA; 1515–1715 AD) in gray.

to long-term mean over larger continental areas in corresponding MCA (LIA) periods (not shown). Our time definition is also in similar range as found for different Northern Hemispheric paleo-reconstructions which were compiled for IPCC (e.g., Jansen et al., 2007). One additional experiment has been performed (PI; 1800–2000 AD) to test the performance of the model to simulate the present-day climate. The sea surface temperature and sea ice cover data have been taken from the AOGCM simulations. The same set of full forcing parameters used for the AOGCM simulations have been applied for our experiments.

2.2. Data

2.2.1. Reconstructions

The AOGCM and AGCM simulated moisture changes between the MCA and LIA are compared with 9 reconstructed paleo-data (Ely et al., 1996; Chauhan et al., 2000; Denniston and Gonzalez, 2000; Kar et al., 2002; Bhattacharya et al., 2007; Sinha et al., 2011a; Ponton et al., 2012; Anoop et al., 2013; Menzel et al., 2013; Sanwal et al., 2013; Prasad et al., 2014; Sarkar et al., 2014) derived from different archives like lake and ocean sediments, peat, and stalagmites (Table 1) using various proxies as pollen, isotopes, mineralogy, and sedimentology. We have evaluated the reliability of the archives using the following criteria: (i) reliability of chronology: the archives should be dated using the radiocarbon or U/Th dating method. We have avoided archives which had the possibility of "hard water effect" where the presence of dead carbon results in artificially old ages for aquatic organic matter (Fontes et al., 1996; Björck and Wohlfarth, 2001); (ii) the proxies used should be sensitive to climate change (Prasad et al., 2014); (iii) the archives should not have long-term (decadal) documented hiatus. Subsequently, we have divided the archives into low, medium, and high confidence categories depending on the number of dates and the sampling (Table 1). The archives in the region (76°E–92°E; 16°N–32°N) encompass sites from both the core monsoon zone (CMZ) and from the northern Himalayan ISM and Westerlies influenced

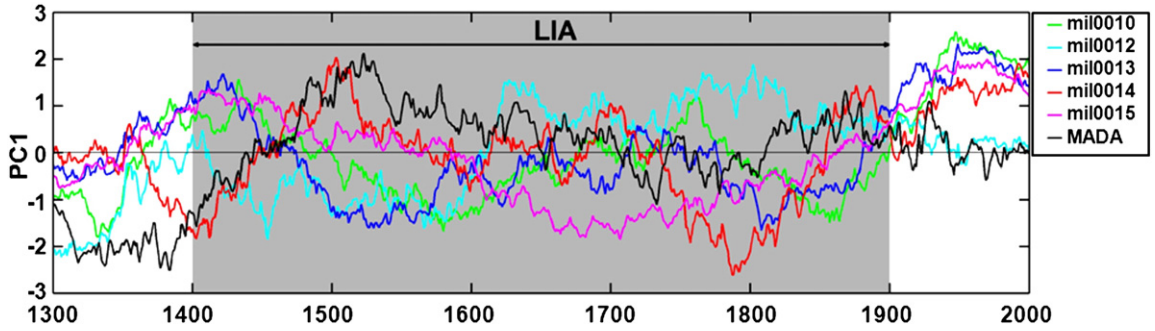

Fig. 2. PC1 time series (101-yr running means) of model derived PDSI for the five ensemble members of the Millennium experiment (Jungclaus et al., 2010) and for the PDSI from MADA (Cook et al., 2010; solid black line) from 1300 to 2000 AD. During the long-term LIA period from 1400 to 1900 AD (gray box) defined by Mann et al. (1999) and Cronin et al. (2003), mil0014 experiment (solid red line) has again, in comparison to all the other ensemble members, the highest positive correlation (0.58) to MADA (thick black line) and a similar trend (Fallah and Cubasch, 2014).

Table 1
Paleoclimatic records from India used in this study. Records are listed from North to South. The colors indicate the confidence level of the records based on chronology and sampling resolution (red = low confidence record with either extrapolated or one date for 1000 years, multi-decadal or higher resolution; orange = medium-range confidence with at least 2 dates and decadal resolution for 1000 years and green = high confidence with more than 2 dates and sub to decadal resolution for 1000 years).

No	Name	ϕ (°N)	λ (°E)	Archive	Proxy	Reference
1	Naychudwari	32.30	77.43	Peat	Pollen	Chauhan et al. (2000)
2	Gangotri	31.00	79.00	Sediment	Pollen	Kar et al. (2002)
3	Dharamjali cave	29.31	80.12	Stalagmite	$\delta^{18}O$, $\delta^{13}C$ Isotopes	Sanwal et al. (2013)
4	Siddi Baba	28.00	84.00	Stalagmite	Laminae thickness	Denniston and Gonzalez, (2000)
5	Paradise Lake	27.30	92.06	Lake sediment	Pollen	Bhattacharya et al. (2007)
6	Narmada basin	23.00	77.43	Fluvial sediment	Flood deposit	Ely et al. (1996)
7	Lonar Lake	19.51	76.00	Lake sediment	Mineralogy and isotope	Anoop et al. (2013) Menzel et al. (2013) Prasad et al. (2014) Sarkar et al. (2014)
8	Dandak + Jhumar	19.00	82.00	Stalagmite	$\delta^{18}O$ Isotope	Sinha et al. (2011a)
9	Godavari	16.00	83.00	Marine sediment	$\delta^{13}C$ of plant waxes	Ponton et al. (2012)

regions (Fig. 3). While the sites in the CMZ are mostly affected by ISM from June to September, the Himalayan records show a seasonality in the moisture source origin between summer (ISM) and winter (Westerlies) due to the northward (southward) shift of the ITCZ band in the corresponding summer (winter) season.

The annual relative moisture signal from the multi-proxy investigations has been translated into a qualitative moisture index using a three-part scale: minus (plus) values indicate drier (wetter) conditions in each 200-yr time slice. "No changes" are marked with zero values. We have also corroborated this reconstruction with the available historical records from Central India, which document decadal scale drought-induced famines during the 13th and 14th centuries AD (Dhavalikar, 1984; Maharatna, 1996).

2.2.2. Observational and reanalysis data

The present-day summer monsoon rainfall pattern over land regions of the PI experiment has been validated with the GPCC5 reanalysis data from Global Precipitation Climatology Centre (Becker et al., 2013) for the period 1901–2000 AD. In this regard, finer-resolved data are remapped on common T31 grid of AOGCM. Additionally, monthly ERA Interim (Dee et al., 2011) wind fields at 850 hPa from 1989 to 2011 AD have been used to verify the lower tropospheric climatological monsoon circulation in summer (Fig. 3).

3. Results

3.1. Present-day monsoon climatology

The simulation of the spatial ISM rainfall patterns over land in AGCM shows better agreement than the simulation of the AOGCM with the observed GPCC5. This is reflected in the pattern correlation coefficient to GPCC5, which is higher for the AGCM (0.72) than for the AOGCM (0.54). Furthermore, pattern standard deviation of AGCM (16.23 mm/day) is closer to GPCC5 (27.17 mm/day) than AOGCM (9.4 mm/day). The rainfall distribution simulated by the AOGCM lacks spatial details, whereas AGCM simulates rainfall belts in regions with complex topography such as the Himalaya more realistically. This is related to a more detailed representation of orographic features in the higher-resolved AGCM.

3.2. Monsoon variability during MCA and LIA

3.2.1. Spatial patterns of annual moisture variations

Our paleoclimate reconstructions (Fig. 4a) indicate a bimodal moisture shift going from the MCA to the LIA. The data are compared with the AOGCM and AGCM simulated "Precipitation minus Evaporation" (P–E) anomalies (Fig. 4a).

The advantage of our higher-resolved AGCM (Fig. 4a; lower panel) in regions with complex topography (Himalaya) is confirmed by a better spatial correspondence with the reconstructed moisture index compared to the coarse resolved AOGCM of the Millennium experiment (Fig. 4a; upper panel). The dipole pattern between wetter (Himalaya) and drier (Central India) conditions is in good agreement between our AGCM simulations and the reconstructions (Fig. 4a; lower panel). Moreover, a strong and statistical significant drying is simulated over the northern Arabian Sea and the Bay of Bengal. The characteristic dipole structure in moisture is further supported by ECMWF climatology for recent times (http://www.ecmwf.int/research/era/ERA-40_Atlas/docs/section_B/parameter_emp.html) indicating realistic patterns in our AGCM compared to coarse resolved AOGCM.

The spatial agreement between model and reconstructions is displayed in a simplified matrix calculating the AOGCM and AGCM simulated moisture signal (P–E) at the site location (Table 2) using a field average over nearest model grid boxes with respect to the geographical coordinates of the record. If field average is higher (lower) than corresponding field standard deviation, then wetter (drier) conditions occur. Field averaged P–E values above (below) 2-sigma field standard deviation threshold indicate stronger (weaker) moisture signals which are coded by different color intensities (Table 2). For AGCM, the Himalayan region generally tends to better spatial resemblance between model and reconstructions compared to Central India indicating a robust moisture signal supported by a statistical significance at 90% confidence level.

3.2.2. Seasonality

3.2.2.1. Moisture variations. In Fig. 4, the summer (JJAS; Fig. 4b) and winter monsoon (DJF; Fig. 4c) P–E anomalies and their statistical significances at 90% confidence level are illustrated for the AOGCM and AGCM simulations between MCA and LIA. Due to better spatial

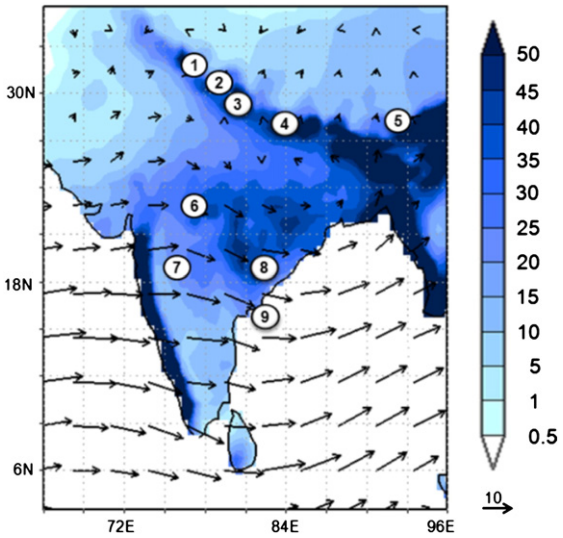

Fig. 3. Study area with cumulated land surface summer monsoon rainfall (JJAS) for GPCC5 dataset from 1901 to 2009 AD (mm/day; colors), summer monsoon (JJAS) lower tropospheric wind vectors at 850 hPa for ERA-Interim reanalysis dataset from 1989 to 2011 AD and the spatial coverage of the Indian paleoclimatic records considered in this study as numbered dots. Numbers of the nodes were assigned according to the geographical coordinates of the respective study site and furthermore refer to the entries in Table 1.

resolution, AGCM shows more detailed representation of seasonal moisture changes.

During summer months MCA tends to be drier compared to LIA especially in a zonal belt from northern Arabian Sea, Central India and northern Bay of Bengal (Fig. 4b; lower panel). Over eastern Himalaya wetter summer conditions occur in "MCA minus LIA". Both regions are statistically significant at 90% confidence level.

During the MCA winter months, the significant drying pattern over Indian Peninsula disappears in comparison to LIA and is restricted over Arabian Sea and Bay of Bengal. Statistically significant wetter conditions "MCA minus LIA" are simulated over western and central Himalaya (Fig. 4c; lower panel).

In addition we calculated the seasonal moisture changes at the 9 reconstruction sites for AGCM as well as for the AOGCM to explain the seasonal variability of the annual signal (Table 2). The sites in Central India, i.e., Lonar, Narmada basin, and Dandak Cave lie in the heart of the Indian summer monsoon region and the signal can be considered as "summer signal" (Table 2). "MCA minus LIA" annual P–E anomalies are more influenced by a winter signal in the western and central Himalayan region, while a summer signal dominates in the eastern Himalaya and Central India.

3.2.2.2. Surface temperatures over land and sea. To understand the physical processes behind the changes in the monsoon circulation, we analyzed the surface temperatures, as the monsoon is mainly driven by the temperature contrast between the Tibetan Plateau and the Indian and Pacific Ocean. The Medieval Climate Anomaly as well as the Little Ice Age have originally been defined after the temperature anomalies experienced during that time over continental regions of the Northern Hemisphere.

The difference in "MCA minus LIA" surface temperatures over the HIMPAC region shows changes within a range of −0.3 and +0.3 K (Fig. 5).

During "MCA minus LIA" summer months (Fig. 5a) a cooling is simulated in northern Arabian Sea, Thar Desert, and the entire Bay of Bengal basin as well as in northeastern India and eastern slopes of the Himalaya. Warmer signals are mostly found over entire India, central and western Himalaya, Indo-Pakistan region, Arabian Peninsula and southern Arabian Sea. The temperature anomalies lead to regional thermal gradients, which are strongest between the northern Arabian Sea and the surrounding land surface regions.

In winter months of "MCA minus LIA" (Fig. 5b) a large cooling area is simulated over the Arabian Peninsula, Gulf of Oman, Indo-Pakistan-region, Himalaya, Tibetan Plateau and northern India. The Indian Ocean basins and southern India show a homogeneous warm pattern in MCA winter. In the two core regions as defined in Table 2, the "MCA minus LIA" summer anomaly exhibits warmer conditions over Central India and western/central Himalaya, and cooler over the eastern Himalaya. MCA calculates generally cooler temperatures over Himalaya and Central India during winter compared to LIA.

3.2.2.3. Vertical integrated moisture fluxes. Fig. 6 illustrates the seasonal moisture flux anomalies "MCA minus LIA" over Monsoon Asia and surrounding ocean basins, which are driven by the regional and remote thermal impact of SST and land surface temperature anomalies. The vertical integrated water vapor content anomalies and wind vectors at 850 hPa are used to describe the dynamical impacts for the anomalous P–E patterns between the MCA and LIA.

The summer months (Fig. 6a) are characterized by a zonal band of negative water vapor anomalies "MCA minus LIA" extending from the Arabian Sea, over the Indian Peninsula and Bay of Bengal toward western Pacific. Contrarily, more water vapor is simulated over the northern and southern part of this zone.

In the winter season (Fig. 6b) the zonal structure of integrated water vapor content "MCA minus LIA" changes to a meridional pattern with strong statistically significant drying over the Arabian Peninsula, Gulf of Oman and Pakistan as well as over the eastern Himalaya and the entire Bay of Bengal, where the drying is more pronounced in winter. Over the Indian subcontinent, central and southern Indian and western Pacific Ocean, large wet patterns are simulated in the MCA compared to LIA. In coherence with regional reduced (increased) low-level winds the large-scale advection of moisture is weakened (enhanced) in the corresponding "MCA minus LIA" season leading to regional P–E anomalies as described in Section 3.2.2.1.

4. Discussion

4.1. Regional moisture inhomogeneity

The annual simulated and reconstructed moisture anomalies "MCA minus LIA" (Fig. 4a; lower panel and Table 2) are more coherent in the Himalaya than over Central India indicating robust signals between MCA and LIA especially in the western and central Himalaya as inferred from statistically significant simulated P–E patterns in this region. Additionally, a higher spatial density of proxies is available for the Himalayan region as compared to Central India.

A pronounced dipole structure "MCA minus LIA" is captured by both the model and data between the two investigated core regions Himalaya (wetter) and Central India (drier). However, spatial inhomogeneity in reconstructed moisture patterns is obvious over Central India, where Lonar Lake indicates a prominent drying trend during the MCA in the CMZ. In contrast, Narmada and Dandak have opposite moisture signals in the MCA compared to LIA. The reconstructed wetter signal at Dandak Cave "MCA minus LIA" corresponds to a regional positive but weak P–E anomaly simulated by AOGCM and AGCM (Table 2). Additional parameters need to be considered while interpreting the dissimilarity of reconstructed moisture signals in the CMZ. The Dandak Cave record (Sinha et al., 2011a) reconstructs droughts based on the oxygen isotope record from the stalagmites using the principle of "amount effect" that assumes that lower (higher) precipitation results in more positive (negative) $\delta^{18}O$ values. However, $\delta^{18}O$ values can also be influenced by changes in storm tracks or source water composition

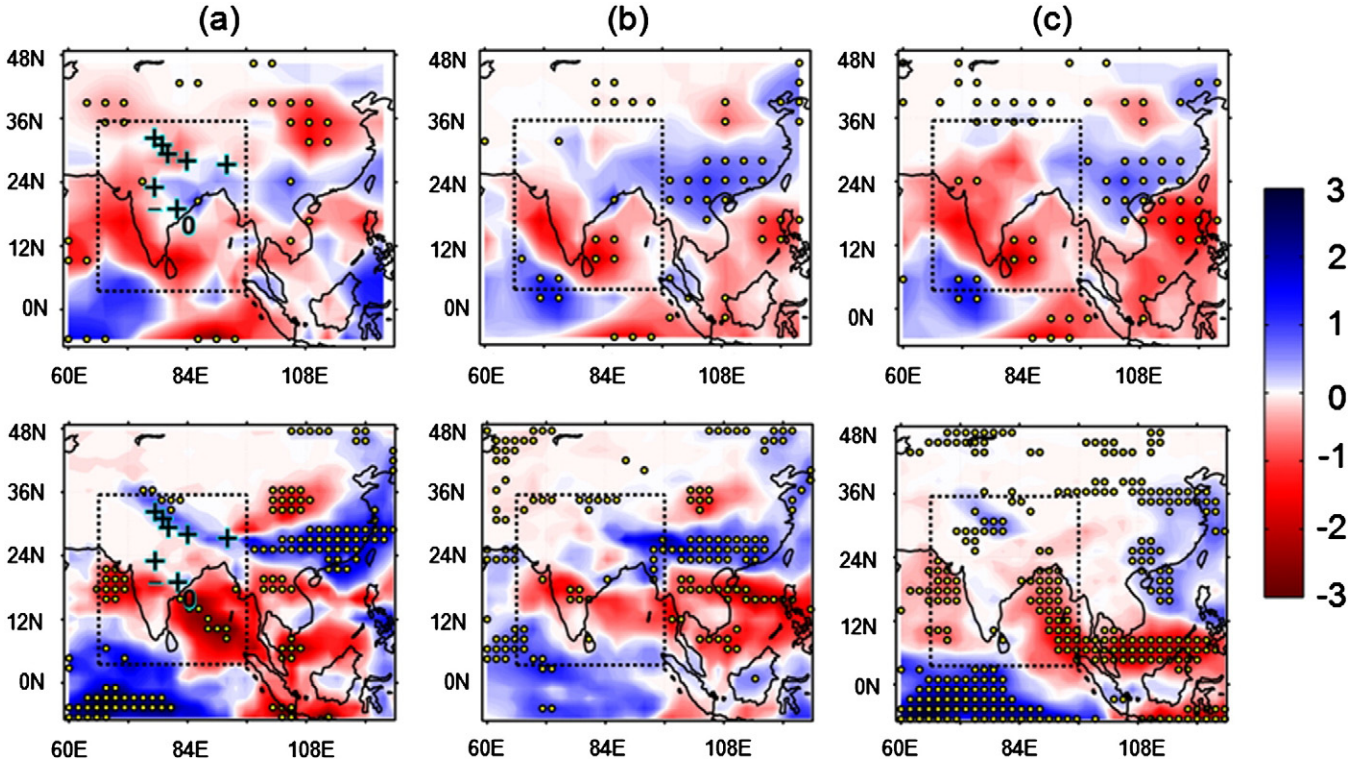

Fig. 4. Simulated anomalies of P–E (mm/day; colors) annual (Fig. 4a), summer monsoon (JJAS; Fig. 4b) and winter monsoon (DJF; Fig. 4c) "MCA minus LIA" for AOGCM (upper panel) and AGCM (lower panel) in Monsoon Asia. In addition the reconstructed moisture index (symbols: "+" wetter, "−" drier and "0" no changes; dimensionless) for "MCA minus LIA" is shown for annual anomalies (Fig. 4a). Statistical significant P–E values ($p < 0.1$; two-tailed *t*-test) are illustrated by yellow dots. The black rectangle box marks the Indian monsoon region on which the study is focused.

(Dayem et al., 2010). Indeed, the multi-proxy record from Lonar Lake does indicate the possibility of past changes in storm tracks in peninsular India (Prasad et al., 2014). The Narmada Valley sediments preserve a record of extreme events, i.e., paleofloods. A comparison of the gauge record for monsoon precipitation from 1948 to 1991 AD with the floods in this valley clearly indicates that the floods do not consistently occur during years of high monsoon precipitation but are more sensitive to the intensity of cyclones (Ely et al., 1996).

Uncertainties leading to model-proxy disagreement are related to errors in reconstructions, limited number of proxies, and our AGCM. (i) The regional dissimilarity of local moisture signals over Central India could be connected to sensitivity of proxies to changes in moisture pathways, and/or intensity rather than amount of precipitation. Lonar in Central India has the advantage of multi-proxy climate reconstruction of hydrological changes within the lake. Since the lake is solely monsoon fed, there is no ambiguity regarding paleoclimate interpretation. (ii) The definition of the correct timing for MCA and LIA epochs in the model is another source of uncertainty. (iii) In addition, the model resolution affects the results. Using higher spatial resolution improves the simulation of the pronounced bimodal moisture pattern between the Himalaya and Central India (Fig. 4).

The study from Dallmeyer et al. (2012) indicates the importance of extending the analysis period of monsoon climate change to other seasons. The paleoclimate moisture reconstructions cannot be used as single indicator for the ISM intensity and the related P–E changes. It has been found that an inhomogeneous seasonal insolation distribution strongly impacts the rainfall throughout the year (Dallmeyer et al., 2012). Since the reconstructed moisture signal is mostly annual, further research has to be done to isolate the seasonality in reconstructions, which will be an important benchmark in improved paleo-reconstruction. In this regard, our model helps to extend the analysis to other seasons and hence provides an added value in past climate research.

4.2. Dynamical drivers for moisture anomalies

Based on our AGCM results we tested the recent paleoclimate network hypothesis of Rehfeld et al. (2013) for ISM–EASM (East Asian Summer Monsoon) connection between MCA and LIA. Compared to this study, our AGCM experiments provide clear advantages of better analysis of the physics behind the moisture changes. The authors suggest that a warmer (cooler) climate leads to stronger zonal ISM penetration into China (stronger meridional EASM and weakened ISM). The linkage between both monsoon systems is governed by northward intrusion (southward retreat) of northern ITCZ as a result of decrease (increase) of Tibetan High in pre-monsoon season. Compared to the LIA, during MCA summer our results show an increase of water vapor and a stronger low-level circulation (Fig. 6a) in a zonal band from the Arabian Peninsula over the Himalaya to eastern China, which can be one indicator for intensification and northern shift of ITCZ during this warm period. The thermal contrast between cooler SSTs in the northern Arabian Sea and warmer land surface over the Indo-Pakistan-region (Fig. 5a) drives the intensification and northward shift of ITCZ. The mean sea level pressure and the geopotential fields at different pressure levels do not reveal significant changes. In our simulation, the strength of the Tibetan High and the location of the ITCZ in pre-monsoon are not altered. Compared to the annual moisture changes "MCA minus LIA" (Fig. 4a; lower panel), summer P–E anomalies do not show signals in central and western Himalaya but more over the eastern Himalaya (Fig. 4b; lower panel). Hence in our model the zonal connection between ISM and EASM during summer as suggested by Rehfeld et al. (2013) is restricted over the eastern Himalaya and eastern China.

The simulated dry anomaly pattern "MCA minus LIA" in the northern Arabian Sea (Fig. 4a; lower panel), which mainly appears in summer (Fig. 4b; lower panel), is related to a SST cooling in this region leading to weaker evaporation of water vapor (Fig. 6a), less upward

Table 2
Simplified matrix of qualitative moisture changes "MCA minus LIA" in Himalaya and Central India for the 9 paleo-records, the "P–E" anomaly of mil0014 member of the Millennium-Experiment (AOGCM; Jungclaus et al., 2010) averaged at site location and the "P–E" anomaly of our AGCM time slice simulations averaged at site location. Annual, summer (JJAS) and winter (DJF) moisture signals are shown. Color cell coding: dark blue (wetter in MCA), light blue (slightly wetter in MCA), orange (slightly drier in MCA), red (drier in MCA) and gray (no available data). Moisture signals taken at site locations which coincide with statistical significant ($p < 0.1$) "P–E" model grid boxes (yellow dots; Fig. 4) are highlighted with circles.

Himalaya				Central India			
Data	Annual	JJAS	DJF	Data	Annual	JJAS	DJF
1. Naychudwari	+			6. Narmada	+	+	
AOGCM	0	+	+	AOGCM	–	0	–
AGCM	+	–	+	AGCM	–	+	0
2. Gangotri	+			7. Lonar	–	–	
AOGCM	0	+	0	AOGCM	–	–	–
AGCM	+	–	+	AGCM	–	–	0
3. Dharamjali	+			8. Dandak/Jhumar	+	+	
AOGCM	–	+	–	AOGCM	+	+	–
AGCM	0	–	+	AGCM	+	+	0
4. Siddi Baba	+			9. Godavari	0		
AOGCM	–	0	–	AOGCM	–	–	–
AGCM	+	+	0	AGCM	–	–	–
5. Paradise Lake	+						
AOGCM	0	+	+				
AGCM	+	+	–				

motion of moist air and reduced precipitation ($P < E$) over this region in MCA summer. Accordingly, a weakening of lower tropospheric large-scale advection of moist air masses embedded in the cross-equatorial southwesterly monsoonal flow results in reduced water vapor content and less summer monsoon precipitation over the Indian Peninsula (Fig. 4b; lower panel) during a warmer climate. This is contrary to the results of Rehfeld et al. (2013), where an intensification of the ISM is presented. The drying in our simulation is amplified by stronger horizontal divergence (not shown), and less cloudiness leads to higher solar radiation input (not shown) and an increase in surface temperatures over India (Fig. 5a).

The dry anomalies "MCA minus LIA" over Indian subcontinent are linked to multi-centennial scale fluctuations of the Indo Pacific Warm Pool (IPWP; Prasad et al., 2014). Our study supports the hypothesis that a long-term intensification of this warm pool (ca. 20°N–15°S; 80°E–160°E) over the last 2000 years together with stronger ENSO and solar activity significantly modulates the ISM intensity. This leads to prolonged drought events over Central India during late Holocene, which are connected to changes in meridional overturning circulation in Indian Ocean and the position of the anomalous Walker cell. This IPWP–ISM connection is well captured by our model. Drying over Central India (Fig. 4a; lower panel) and warm annual SST anomalies in the IPWP region (not shown) are simulated. Stronger El Niño–monsoon linkage "MCA minus LIA" is not seen in AGCM. In this regard, other AOGCM studies with prescribed warm pool would be more appropriate to simulate the effect of IPWP and ENSO more realistically.

Over the Bay of Bengal the zonal drying band continues to be influenced by SST cooling and reduced moisture flux. Wetter "MCA minus LIA" summer conditions ($P > E$) are shown for Bangladesh and especially for the eastern Himalaya (Fig. 4b; lower panel), which are driven by (i) strong thermal contrast between warmer Indian subcontinent and cooler ocean (Fig. 5a) leading to an enhanced northern penetration of moist air masses toward the eastern Himalayan region. Orographic uplifting results in higher precipitation at the southern slopes. (ii) Further, moist air masses from eastern China, where a stronger EASM is simulated during MCA (Rehfeld et al., 2013), penetrate westwards to the eastern Himalaya within a stronger moisture advection at 850 hPa (Fig. 5a). The stronger ISM in eastern Himalaya is embedded in the zonal monsoon intensification north of 25°N as discussed in Rehfeld et al. (2013). The higher summer precipitation in this region influences the surface cooling (Fig. 5a) due to evaporation.

In winter season the changes in western and central Himalaya are more obvious (Fig. 4c; lower panel) due to the effect of westerly induced precipitation events in association with orographic uplifting (e.g., Bookhagen and Burbank, 2010). A strong homogeneous cooling area is simulated in "MCA minus LIA" winter from the Arabian Sea, over Indo-Pakistan-region toward the Himalaya. It encompasses northern India (Fig. 5b) in accordance with stronger near-surface southerly advection of cold and dry air masses that originated in Siberian High (Fig. 6b). A small region over India shows higher water vapor content in MCA winter, which is transported to the equatorial ITCZ. Windward

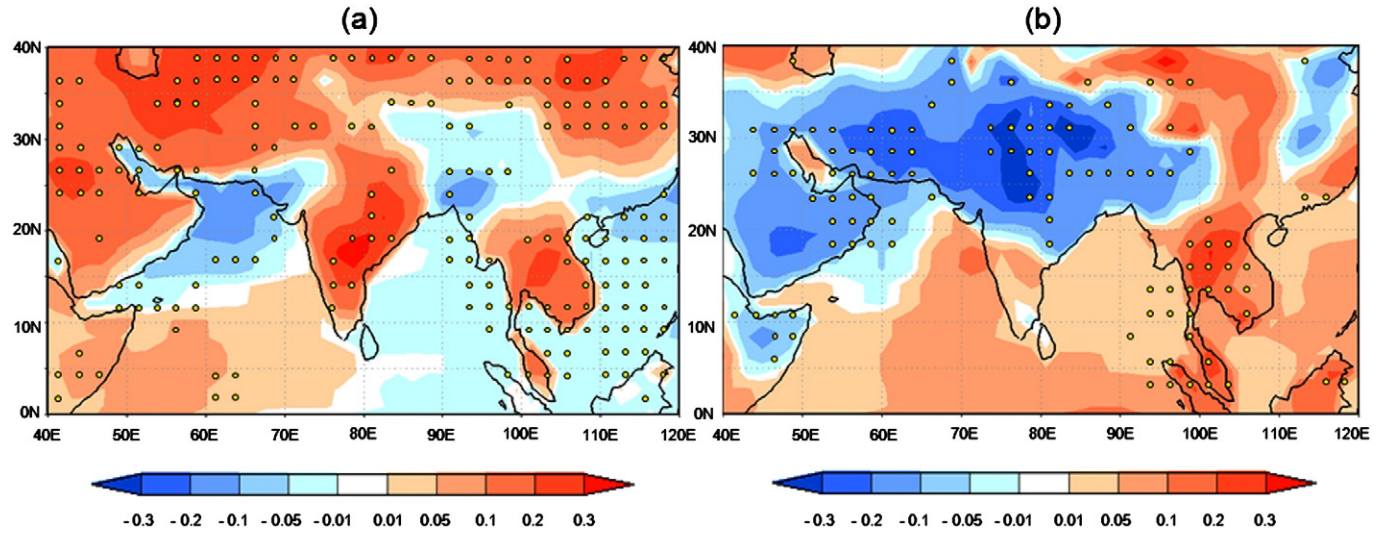

Fig. 5. Anomalies of surface temperatures over land and SST (°C; colors) during summer (JJAS; Fig. 5a) and winter (DJF; Fig. 5b) for AGCM "MCA minus LIA". Statistical significant values ($p < 0.1$; two-tailed *t*-test) are illustrated by yellow dots.

of Sri Lanka and southeastern India, orographic uplifting leads to slightly wetter "MCA minus LIA" conditions. Near the equator the ITCZ rainfall belt depicts wetter conditions in "MCA minus LIA" winter (Fig. 4c; lower panel) in association with SST warming and regional convection of evaporated water vapor, which is much stronger in that region (Fig. 6b). The drying area in the Bay of Bengal is larger due to weaker vertical integrated water vapor content, reduced moisture fluxes (Fig. 6b) and stronger horizontal divergence (not shown).

Finally the interpretation of physical drivers shows that we can isolate three spatial clusters within the ISM realm leading to summer and winter moisture anomalies: (i) western and central Himalaya influenced by changes in intensity of extra-tropical Westerlies during winter, (ii) the eastern Himalaya influenced by summer variations of thermal contrast between Bay of Bengal and Indian land surface as well as by the zonal band of intensified ISM–EASM link as suggested by Rehfeld et al. (2013), and (iii) Central India with impact of summer moisture anomalies affected by the thermal SST signal in northern Arabian Sea, the corresponding strength of the large-scale advection of moist air masses toward India, and the IPWP–ISM link on longer time scales.

5. Conclusions

The general atmospheric circulation model ECHAM5 has been used to simulate the Indian Monsoon Variability within the last Millennium. The focus was on 200-yr-long time slices of the Medieval Climate Anomaly (900–1100 AD) and the Little Ice Age (1515–1715 AD).

Simulated and reconstructed annual moisture signals agree over the Himalaya and Central India. The numerous archives in the Himalaya region exhibit a high consistency with the model data in describing past moisture changes. In Central India, where less proxy data are available to describe the moisture distribution in the heterogeneous topography, the agreement is only prominent in summer. The proxy data are anchored around the new Lonar Lake record, which due to its long chronology and multi-proxy reconstruction is representative for the

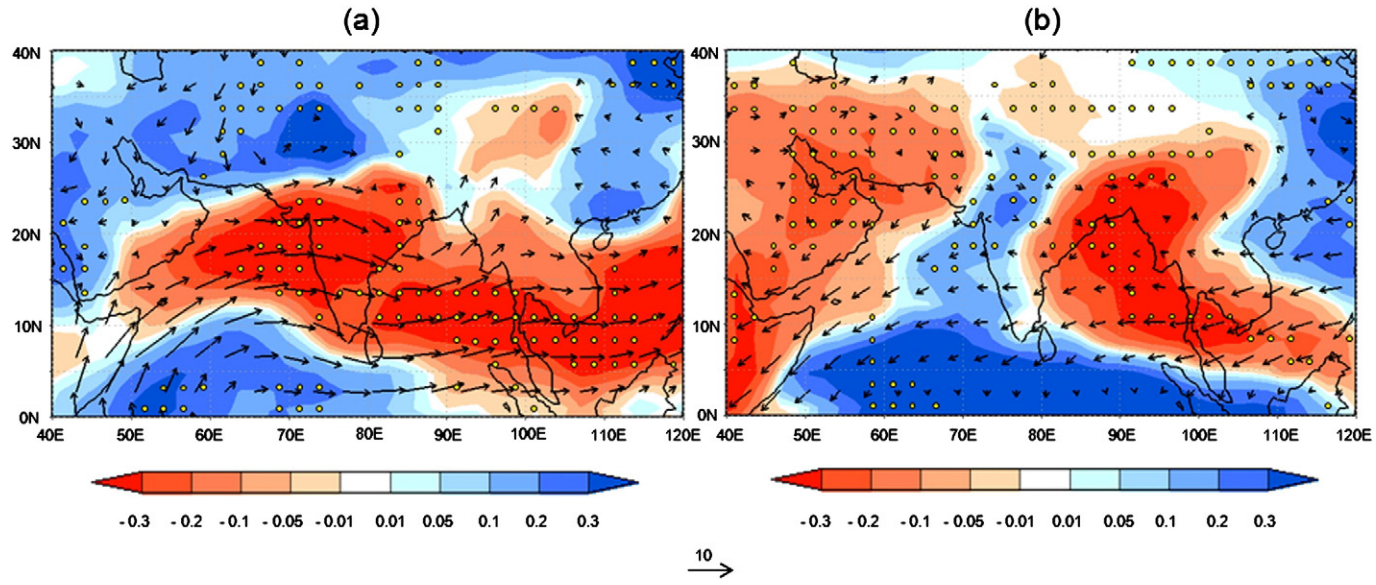

Fig. 6. Anomalies of vertical integrated water vapor (kg/m^2; colors) and wind vectors at 850 hPa during summer (JJAS; Fig. 6a) and winter (DJF; Fig. 6b) for AGCM "MCA minus LIA". Statistically significant values of vertical integrated water vapor ($p < 0.1$; two-tailed *t*-test) are illustrated by yellow dots.

paleo-hydrological changes in Central India. This record has been cross-validated with historical data for the investigated time interval (Prasad et al., 2014).

Between the warmer (MCA) and colder (LIA) climate epochs a distinct dipole pattern has been identified between the Himalaya and Central India. These annual moisture anomalies between the MCA and LIA show a seasonal dependence. The summer months contribute more to the annual signal than the winter months. The intensive wet pattern in the Himalaya has generally decreased in both seasons. During summer (winter) months of the warmer medieval period the model simulated higher P–E values over the eastern (western) parts as compared to LIA. The dry anomaly over Central India is more striking in MCA summer.

We tested the hypothesis that a warmer (cooler) climate leads to stronger (weaker) ISM as proposed by Rehfeld et al. (2013) and analyzed the physical processes connected to this response. We extended Rehfeld's theory and identified three larger regions within the ISM region which have pronounced moisture anomalies in summer and winter: (i) western and central Himalaya, which is influenced by variations in intensity of extra-tropical Westerlies during winter, (ii) the eastern Himalaya which in summer is affected by changes in thermal gradient between the Bay of Bengal and the Indian subcontinent as well as by the zonal band of strengthened ISM–EASM link, and (iii) Central India whose summer moisture anomalies are affected by the SST pattern in northern Arabian Sea. As Prasad et al. (2014) pointed out, the strength in the large-scale advection of moist air masses toward India and the Indo Pacific Warm Pool–ISM link varies on a multi-centennial time scale. Compared to Rehfeld et al. (2013) our "MCA minus LIA" anomalies showed a northern shift in ISM activity leading to weakening (enhancement) of ISM rainfall over Central India (eastern Himalaya) during warmer climate.

Our results indicate that the combination of proxy and model data leads to an improved understanding of the paleo-climate. Proxy data are used to validate model simulations of climates of the past. The model data can then be analyzed to investigate the mechanism behind the changes.

Acknowledgments

This research was supported and funded by the DFG research group FOR 1380 "HIMPAC" and the German Federal Ministry of Education and Research (BMBF) research project "CADY" as part of the joint research program "CAME — Central Asia: Monsoon Dynamics and Geo-Ecosystems". The authors thank the individual HIMPAC and CADY/CAME teams for permanent support and fruitful discussions, especially Ilona Jördis Jäkel and Katharina Lange for helping us in the preparation of the figures. Further we thank Dr. Raghavan Krishnan and Dr. Milind Mujumdar from the Indian Institute of Tropical Meteorology (IITM), Pune for enhanced collaboration and interesting discussions within HIMPAC and for their hospitality during a research stay at IITM. The COSMOS data from the Millennium experiment had been supplied by the Max Planck Institute for Meteorology (MPI-M) Hamburg. The authors thank Dr. Johann H. Jungclaus, MPI-M Hamburg for COSMOS data from the Millennium experiment and Dr. Anne Dallmeyer, MPI-M Hamburg for many helpful advices in SST interpolation and running ECHAM5 model. Computational resources were made available by the German Climate Computing Center (DKRZ) through support from the BMBF. Finally we acknowledge the critical comments of the anonymous reviewer, who improved and clarified the manuscript.

Appendix A. Supplementary data

Supplementary data to this article can be found online at http://dx.doi.org/10.1016/j.gloplacha.2014.08.016.

References

Anandhi, A., Nanjundiah, R.S., 2014. Performance evaluation of AR4 Climate Models in simulating daily precipitation over the Indian region using skill scores. Theor. Appl. Climatol. http://dx.doi.org/10.1007/s00704-013-1043-5 (16 pp.).

Anoop, A., Prasad, S., Plessen, B., Basavaiah, N., Gaye, B., Naumann, R., Menzel, P., Weise, S., Brauer, A., 2013. Palaeoenvironmental implications of evaporative gaylussite crystals from Lonar Lake, central India. J. Quat. Sci. 28, 349–359.

Becker, A., Finger, P., Meyer-Christoffer, A., Rudolf, B., Schamm, K., Schneider, U., Ziese, M., 2013. A description of the global land-surface precipitation data products of the Global Precipitation Climatology Centre with sample applications including centennial (trend) analysis from 1901–present. Earth Syst. Sci. Data 5, 71–99.

Bhattacharya, A., Sharma, J., Shah, S.K., Chaudhary, V., 2007. Climatic changes during the last 1800 yrs BP from Paradise Lake, Sela Pass, Arunachal Pradesh, Northeast Himalaya. Curr. Sci. 93 (7), 983–987.

Björck, S., Wohlfarth, B., 2001. ^{14}C chronostratigraphic techniques in paleolimnology. In: Last, W.M., Smol, J.P. (Eds.), Tracking Environmental Change Using Lake SedimentsBasin Analysis, Coring, and Chronological Techniques. vol. 1. Kluwer, Dordrecht, pp. 205–245.

Bookhagen, B., Burbank, D.W., 2010. Toward a complete Himalayan hydrological budget: spatiotemporal distribution of snowmelt and rainfall and their impact on river discharge. J. Geophys. Res. 115. http://dx.doi.org/10.1029/2009JF001426.

Borgaonkar, H.P., Sikdera, A.B., Rama, S., Panta, G.B., 2010. El Niño and related monsoon drought signals in 523-year-long ring width records of teak (*Tectona grandis* L. F.) trees from south India. Palaeogeogr. Palaeoclimatol. Palaeoecol. 285, 74–84.

Bretagnon, P., Francou, G., 1988. Planetary theories in rectangular and spherical variables — VSOP 87 solutions. Astron. Astrophys. 202, 309–315.

Chauhan, M.S., Mazari, R.K., Rajagopalan, G., 2000. Vegetation and climate in upper Spiti region, Himachal Pradesh during late Holocene. Curr. Sci. 79 (3), 373–377.

Clift, P.D., Plumb, R.A., 2008. The Asian Monsoon: Causes, History and Effects. Cambridge University Press, Cambridge.

Cook, E.R., Anchukaitis, K.J., Buckley, B.M., D'Arrigo, R.D., Jacoby, G.C., Wright, W.E., 2010. Asian monsoon failure and megadrought during the last millennium. Science 328, 486–489.

Cronin, T.M., Dwyer, G.S., Kamiya, T., Schwede, S., Willard, D.A., 2003. Medieval Warm Period, Little Ice Age and 20th century temperature variability from Chesapeake Bay. Glob. Planet. Chang. 36, 17–29.

Crowley, T.J., Zielinski, G., Vinther, B., Udisti, R., Kreutz, K., Cole-Dai, J., Castellano, J., 2008. Volcanism and the Little Ice Age. PAGES Newsl. 16, 22–23.

Dai, A., Trenberth, K.E., Qian, T., 2004. A global dataset of Palmer Drought Severity Index for 1870–2002: relationship with soil moisture and effects of surface warming. J. Hydrometeorol. 5, 1117–1130.

Dallmeyer, A., Claussen, M., Wang, Y., Herzschuh, U., 2012. Spatial variability of Holocene changes in the annual precipitation pattern: a model-data synthesis for the Asian monsoon region. Clim. Dyn. 39, 18.

Dayem, K., Molnar, P., Battisti, D., Roe, G., 2010. Lessons learned from oxygen isotopes in modern precipitation applied to interpretation of speleothem records of paleoclimate from eastern Asia. Earth Planet. Sci. Lett. 295, 219–230.

Dee, D.P., Uppala, S.M., Simmons, A.J., Berrisford, P., Poli, P., Kobayashi, S., Andrae, U., Balmaseda, M.A., Balsamo, G., Bauer, P., Bechtold, P., Beljaars, A.C.M., van de Berg, L., Bidlot, J., Bormann, N., Delsol, C., Dragani, R., Fuentes, M., Geer, A.J., Haimberger, L., Healy, S.B., Hersbach, H., Hólm, E.V., Isaksen, L., Kållberg, P., Köhler, M., Matricardi, M., McNally, A.P., Monge-Sanz, B.M., Morcrette, J.-J., Park, B.-K., Peubey, C., de Rosnay, P., Tavolato, C., Thépaut, J.-N., Vitart, F., 2011. The ERA-Interim reanalysis: configuration and performance of the data assimilation system. Q. J. R. Meteorol. Soc. 137, 553–597.

Denniston, R.F., Gonzalez, L.A., 2000. Speleothem evidence for changes in Indian summer monsoon precipitation over the last ~2300 years. Quat. Res. 53, 196–202.

Dhavalikar, M.K., 1984. Toward an ecological model for chalcolithic cultures of central and western India. J. Anthropol. Archaeol. 3, 133–158.

Ding, Y.H., 2007. The variability of the Asian summer monsoon. J. Meteorol. Soc. Jpn. 85, 21–54.

Ely, L.L., Enzel, Y., Baker, V.R., Kale, V.S., Mishra, S., 1996. Changes in the magnitude and frequency of late Holocene monsoon floods on the Narmada River, central India. Geol. Soc. Am. Bull. 108 (9), 1134–1148.

Fallah, B., Cubasch, U., 2014. A comparison of model simulations of Asian mega-droughts during the past millennium with proxy reconstructions. Clim. Past Discuss. 10, 2685–2716.

Fleitmann, D., Burns, S.J., Mangini, A., Mudelsee, M., Kramers, J., Villa, I., Neff, U., Subbary, A.-A., Buettner, A., Hippler, D., Matter, A., 2007. Holocene ITCZ and Indian monsoon dynamics recorded in stalagmites from Oman and Yemen (Socotra). Quat. Sci. Rev. 26, 170–188.

Fontes, J.C., Gasse, F., Gibert, E., 1996. Holocene environmental changes in Bangong Co Basin (Western Tibet): part 1. Chronology and stable isotopes of carbonates of a Holocene lacustrine core. Palaeogeogr. Palaeoclimatol. Palaeoecol. 120, 25–47.

Fortuin, J.P.F., Kelder, H., 1998. An ozone climatology based on ozone sonde and satellite measurements. J. Geophys. Res. 103, 31709–31734.

Gadgil, S., 2003. The Indian monsoon and its variability. Annu. Rev. Earth Planet. Sci. 31, 429–467.

Graham, N.E., Ammann, C.M., Fleitmann, D., Cobb, K.M., Luterbacher, J., 2010. Support for global climate reorganization during the "Medieval Climate Anomaly". Clim. Dyn. 37, 1217–1245.

Grove, J.M., 1988. The Little Ice Age. Menthuen, London.

Jansen, E., Overpeck, J., Briffa, K., Duplessy, J.-C., Joos, F., Masson-Delmotte, V., Olago, D., Otto-Bliesner, B., Peltier, W., Rahmstorf, S., Ramesh, R., Raynaud, D., Rind, D., Solomina, O., Villalba, R., Zhang, D., 2007. Paleoclimate. In: Solomon, S., Qin, D.,

Manning, M., Chen, Z., Marquis, M., Averyt, K., Tignor, M., Miller, H. (Eds.), Climate change 2007: the physical science basisContribution of working group 1 to the Fourth Assessment Report of the Intergovernmental Panel on Climate Change. Cambridge University Press, Cambridge, pp. 433–497.
Jones, P.D., Osborn, T.J., Briffa, K.R., 2001. The evolution of climate over the last millennium. Science 292, 662–667.
Jungclaus, J.H., Lorenz, S.J., Timmreck, C., Reick, C.H., Brovkin, V., Six, K., Segschneider, J., Giorgetta, M.A., Crowley, T.J., Pongratz, J., Krivova, N.A., Vieira, L.E., Solanki, S.K., Klocke, D., Botzet, M., Esch, M., Gayler, V., Haak, H., Raddatz, T., Roeckner, E., Schnur, R., Widmann, H., Claussen, M., Stevens, B., Marotzke, J., 2010. Climate and carbon-cycle variability over the last millennium. Clim. Past 6, 723–737.
Kar, R., Ranhotra, P.S., Bhattacharyya, A., Sekar, B., 2002. Vegetation vis-a-vis climate and glacial fluctuations of the Gangotri glacier since the last 2000 years. Curr. Sci. 82 (3), 347–351.
Krishna Kumar, K., Hoerling, M., Rajagopalan, B., 2005. Advancing dynamical prediction of Indian monsoon rainfall. Geophys. Res. Lett. 32, L08704.
Krishnan, R., Kumar, V., Sugi, M., Yoshimura, J., 2009. Internal feedbacks from monsoon–midlatitude interactions during droughts in the Indian summer monsoon. J. Atmos. Sci. 66, 553–578.
Krivova, N.A., Balmaceda, L., Solanki, S.K., 2007. Reconstruction of solar total irradiance since 1700 from the surface magnetic flux. Astron. Astrophys. 467, 335–346.
Lamb, H.H., 1965. The early medieval warm epoch and its sequel. Palaeogeogr. Palaeoclimatol. 1, 13–37.
Liu, X., Dong, H., Yang, X., Herzschuh, U., Zhang, E., Stuut, J.-B.W., Wang, Y., 2009. Late Holocene forcing of the Asian winter and summer monsoon as evidenced by proxy records from the northern Qinghai–Tibetan Plateau. Earth Planet. Sci. Lett. 280 (1), 276–284.
Maharatna, A., 1996. The Demography of Famines: An Indian Historical Perspective. Oxford University Press, Delhi.
Mann, M.E., Bradley, R.S., Hughes, M.K., 1999. Northern Hemisphere temperatures during the past millennium: inferences, uncertainties, and limitations. Geophys. Res. Lett. 26, 759–762.
Marland, G., Boden, T.A., Andres, R.J., 2003. Global, regional and national fossil fuel CO_2 emissions. In: US Department of Energy (Ed.), Trends: A Compendium of Data on Global Change. Carbon Dioxide Information Analysis Center, Oak Ridge National Laboratory, Oak Ridge.
Marsland, S.J., Haak, H., Jungclaus, J.H., Latif, M., Röske, F., 2003. The Max-Planck-Institute global ocean/sea ice model with orthogonal curvilinear coordinates. Ocean Model. 5 (2), 91–127.
Meehl, G.A., Arblaster, J.M., Matthes, K., Sassi, F., van Loon, H., 2009. Amplifying the Pacific climate system response to a small 11-year solar cycle forcing. Science 325, 1114–1118.
Menzel, P., Gaye, B., Wiesner, M., Prasad, S., Stebich, M., Das, B.K., Anoop, A., Riedel, N., Basavaiah, N., 2013. Influence of bottom water anoxia on nitrogen isotopic ratios and amino acid contributions of recent sediments from small eutrophic Lonar Lake, central India. Limnol. Oceanogr. 58, 1061–1074.
Polanski, S., Rinke, A., Dethloff, K., 2010. Validation of the HIRHAM-simulated Indian summer monsoon circulation. Adv. Meteorol. 2010. http://dx.doi.org/10.1155/2010/415632 (14 pp.).
Polanski, S., Rinke, A., Dethloff, K., Lorenz, S.J., Wang, Y., Herzschuh, U., 2012. Simulation of the mid-Holocene Indian summer monsoon circulation with a regional climate model. Open Atmos. Sci. J. 6, 42–48.
Pongratz, J., Reick, C.H., Raddatz, T., Claussen, M., 2008. A reconstruction of global agricultural areas and land cover for the last millennium. Global Biogeochem. Cycles 22, GB3018. http://dx.doi.org/10.1029/2007GB003153.
Ponton, C., Giosan, L., Eglinton, T.I., Fuller, D.Q., Johnson, J.E., Kumar, P., Collett, T.S., 2012. Holocene aridification of India. Geophys. Res. Lett. 39, L03704.
Prasad, S., Enzel, Y., 2006. Holocene paleoclimates of India. Quat. Res. 66 (3), 442–453.
Prasad, S., Anoop, A., Riedel, N., Sarkar, S., Menzel, P., Basavaiah, N., Krishnan, R., Fuller, D., Plessen, B., Gaye, B., Röhl, U., Wilkes, H., Sachse, D., Sawant, R., Wiesner, B., Stebich, M., 2014. Prolonged monsoon droughts and links to Indo-Pacific warm pool: a Holocene record from Lonar Lake, Central India. Earth Planet. Sci. Lett. 391, 171–182.
Raddatz, T.J., Reick, C.H., Knorr, W., Kattge, J., Roeckner, E., Schnur, R., Schnitzler, K.-G., Wetzel, P., Jungclaus, J.H., 2007. Will the tropical land biosphere dominate the climate-carbon cycle feedback during the twenty-first century? Clim. Dyn. 29 (6), 565–574.
Rehfeld, K., Marwan, N., Breitenbach, S.F.M., Kurths, J., 2013. Late Holocene Asian summer monsoon dynamics from small but complex networks of paleoclimate data. Clim. Dyn. 41, 3–19.
Roeckner, E., Bäuml, G., Bonaventura, L., Brokopf, R., Esch, M., Giorgetta, M., Hagemann, S., Kirchner, I., Kornblueh, L., Manzini, E., Rhodin, A., Schlese, U., Schulzweida, U., Tompkins, A., 2003. The atmospheric general circulation model ECHAM 5 PART 1: model description. Technical report 349. Max-Planck-Institute for Meteorology (140 pp.).
Sanwal, J., Singh Kotlia, B., Rajendran, C., Masood Ahmad, S., Rajendran, K., Sandiford, M., 2013. Climatic variability in Central Indian Himalaya during the last ~1800 years: evidence from a high resolution speleothem record. Quat. Int. 304, 183–192.
Sarkar, S., Wilkes, H., Prasad, S., Brauer, A., Riedel, N., Stebich, M., Basavaiah, N., Sachse, D., 2014. Spatial heterogeneity of lipid biomarker distributions in the catchment and sediments of a crater lake in central India. Org. Geochem. 66, 125–136.
Schurer, A.P., Tett, S.F.B., Hegerl, G.C., 2014. Small influence of solar variability on climate over the past millennium. Nat. Geosci. 7, 104–108.
Sengupta, S., Sarkar, A., 2006. Stable isotope evidence of dual (Arabian and Bay of Bengal) vapour sources in monsoonal precipitation over north India. Earth Planet. Sci. Lett. 250, 511–521.
Shaw, R., Nguyen, H., 2011. Droughts in Asian Monsoon Region, Community, Environment and Disaster Risk Management 8. Emerald Books, Kyoto University, Kyoto.
Sinha, A., Berkelhammer, M., Stott, L., Mudelsee, M., Cheng, H., Biswas, J., 2011a. The leading mode of Indian Summer Monsoon precipitation variability during the last millennium. Geophys. Res. Lett. 38, L15703.
Sinha, A., Stott, L., Berkelhammer, M., Cheng, H., Lawrence Edwards, R., Buckley, B., Aldenderfer, M., Mudelsee, M., 2011b. A global context for megadroughts in monsoon Asia during the past millennium. Quat. Sci. Rev. 30, 47–62.
Solanki, S.K., Usoskin, I.G., Kromer, B., Schuessler, M., Beer, J., 2004. Unusual activity of the Sun during recent decades compared to the previous 11,000 years. Nature 431, 1084–1087.
Tanre, D., Geleyn, J.-F., Slingo, J.M., 1984. First results of the introduction of an advanced aerosol–radiation interaction in the ECMWF low resolution global model. In: Gerber, H., Deepak, A. (Eds.), Aerosols and Their Climatic Effects. Deepak Publishing, Hampton, pp. 133–177.
Ummenhofer, C.C., D'Arrigo, R.D., Anchukaitis, K.J., Buckley, B.M., Cook, E.R., 2012. Links between Indo-Pacific climate variability and drought in the Monsoon Asia Drought Atlas. Clim. Dyn. 39, 16.
Wang, B., 2006. The Asian Monsoon. Springer/Praxis Publishing Co., Berlin.
Wang, B., Wu, R., Lau, K.M., 2001. Interannual variability of the Asian summer monsoon: contrasts between the Indian and the Western North Pacific-East Asian Monsoon. J. Clim. 14, 4073–4090.
Wang, Y., Liu, X., Herzschuh, U., 2010. Asynchronous evolution of the Indian and East Asian Summer Monsoon indicates by Holocene moisture pattern in monsoonal Central Asia. Earth Sci. Rev. 103, 135–153.
Webster, P.J., Magana, V.O., Palmer, T.N., Shukla, J., Tomas, R.T., Yanai, M., Yasunari, T., 1998. Monsoons: processes, predictability and the prospects of prediction. J. Geophys. Res. 103, 14451–14510.
Wetzel, P., Maier-Reimer, E., Botzet, M., Jungclaus, J.H., Keenlyside, N., Latif, M., 2006. Effects of ocean biology on the penetrative radiation in a coupled climate model. J. Clim. 19, 3973–3987.